Surface & Coatings Technology 344 (2018) 596–600

Contents lists available at ScienceDirect

Surface & Coatings Technology

journal homepage: www.elsevier.com/locate/surfcoat

Structure and optical properties of SiO_2 films with ZnSe nanocrystals formed by ion implantation

Maksim Makhavikou[a], Fadei Komarov[a], Irina Parkhomenko[b], Liudmila Vlasukova[b], Oleg Milchanin[a], Jerzy Żuk[c,*], Elke Wendler[d], Ivan Romanov[b], Olga Korolik[b], Altynai Togambayeva[e]

[a] Institute of Applied Physics Problems, Kurchatov Str. 7, 220045 Minsk, Belarus
[b] Belarusian State University, Nezavisimosti Ave. 4, 220030 Minsk, Belarus
[c] Institute of Physics, Maria Curie-Skłodowska University, pl. M. Curie-Skłodowskiej 1, 20-031 Lublin, Poland
[d] Friedrich-Schiller University Jena, Max-Wien-Platz 1, D-07743 Jena, Germany
[e] Al-Farabi Kazakh National University, Al-Farabi Ave. 71, Almaty 050040, Kazakhstan

ARTICLE INFO

Keywords:
ZnSe nanocrystals
SiO_2 films
Ion implantation
XTEM
Photoluminescence
Quantum size effect

ABSTRACT

ZnSe nanocrystals have been formed in the silicon dioxide matrix by the sequential high-fluence implantation of Zn^+ and Se^+ ions at 500 °C. After implantation a part of samples was annealed at 1000 °C for 3 min using rapid thermal annealing. Structural and optical properties of ZnSe/SiO_2 nano-composite films were analyzed by means of Rutherford Backscattering Spectrometry, cross-sectional Transmission Electron Microscopy, Raman scattering and photoluminescence techniques. It was shown that a sequence of implantation affects structural and optical properties of synthesized ZnSe clusters. Based on the Raman scattering and photoluminescence data the samples for which Zn ions were implanted first exhibited a better ZnSe crystalline quality than those of reverse sequence of implantation, i.e. with Se ions implanted at the beginning. The bands of blue ZnSe band edge emission and green-red ZnSe deep defect level emission were revealed in the PL spectra of the as-implanted and annealed nano-composites. The PL spectral features observed in the blue region are due to the quantum-size effects in the ZnSe nanocrystals embedded into the silicon dioxide matrix. The PL intensity ratio of the deep defect band to the near edge emission is higher in the samples first implanted with Se ions, and Zn ions implanted next. The effect of rapid thermal annealing on structural and light-emitting properties was discussed.

1. Introduction

Selenide-based nanostructural materials, such as wide-band gap A_2B_6 semiconductors, have been studied intensively due to their wide variety of practical application in the fields of light-emitting devices, solar cells, sensors, and optical recording materials. Following the demonstration of possible application of zinc selenide in photoelectronic devices, an intensive attention is paid to ZnSe as an alternative to the more toxic Cd-based materials. Indeed, ZnSe-based materials in such forms as thin films, nanocrystals (NCs), quantum wells, flower-shaped nanocrystals [1], nanoribbons [2], nanowires [3], hollow microspheres [4] and bulk crystals are applicable for fabrication of blue and green light-emitting diodes due to the direct band gap, infrared windows due to wide transmission wavelength range, lenses and prisms, and optically controlled switching devices due to giant photoresistivity.

Numerous investigations were focused on the synthesis of high-quality ZnSe nanocrystals (NCs). In most cases NCs were formed by a multistep chemical route [5–10]. For practical applications, however, the ion beam technique is very promising due to its compatibility to the common Si technology. Ion implantation is a suitable method of synthesis of nanostructured films and NCs embedded in different dielectric and semiconductor matrices. Formation of A_2B_6 nanocrystals such as CdS, CdSe, ZnS, ZnO [11–14] using ion implantation was previously reported. To our best knowledge, up to now no reports have been published on the ion-beam synthesis of ZnSe nanocrystals in SiO_2 layers except a brief notice in [15] concerning possibility of ZnSe precipitates creation in a-SiO_2. In this paper structural and optical properties of ZnSe nanocrystals synthesized in the amorphous SiO_2 matrix by ion implantation were studied.

* Corresponding author.
E-mail address: jotzet@hektor.umcs.lublin.pl (J. Żuk).

https://doi.org/10.1016/j.surfcoat.2018.03.017
Received 31 October 2017; Received in revised form 5 March 2018; Accepted 8 March 2018
Available online 21 March 2018

2. Material and methods

The $1 \times 1\,cm^2$ samples were cut from the thermally oxidized Si (100) wafer. According to Cross-sectional Transmission Electron Microscopy (XTEM), the thickness of SiO_2 film was 600 nm. Afterwards, these samples were sequentially "hot" implanted with Zn^+ and Se^+ ions at a target temperature of 500 °C. The energies of ions (150 keV for Zn^+ and 170 keV for Se^+) were chosen based on the computer simulation (TRIM code) to obtain overlapping concentration profiles of Zn and Se species. Both types of ions were implanted with the same fluence of 4×10^{16} ions/cm^2.

Two sets of samples were prepared. Those of the first set (samples A) were implanted at first with Zn ions and after that with Se ions. In the other set (samples B) the order of Zn and Se implantations was inverted. Rapid thermal annealing (RTA) at 1000 °C for 3 min in Ar atmosphere was performed on a part of the implanted samples. Rutherford Backscattering Spectrometry (RBS) using 2.5 MeV He^+ ions was employed to study the elemental composition of the implanted oxide films. The chosen energy of He ions was high enough to resolve Zn and Se peaks in the RBS spectra. Phase composition of the samples was investigated by means of Raman scattering (RS). RS measurements were performed in backscattering geometry with a Nanofinder High End micro-Raman spectrometer (LOTIS TII) using a 532-nm laser beam as the excitation source. Structural composition was studied by the cross-section technique of Transmission Electron Microscopy (XTEM) with a Hitachi H-800 electron microscope operating at 200 keV. Photoluminescence (PL) spectra were registered at room temperature using the He-Cd laser beam at the wavelength $\lambda = 325$ nm as the excitation source.

3. Results and discussion

Fig. 1 shows the impurity concentration profiles in SiO_2 calculated from the experimental RBS spectra for the as-implanted and annealed samples. The Zn and Se concentration profiles maxima simulated with TRIM are located at comparable depths near 112–114 nm (not shown in Figure). However, the maxima of concentration profiles of "hot" implanted impurities calculated from the experimental RBS spectra are shifted to the surface in comparison with the simulated ones. Thus in the case of the sample A (Fig. 1a), the "experimental" maxima of the Zn and Se concentration profiles are located at the depth of ~70 and 90 nm, respectively. For the sample B (Fig. 1b), the maxima of the Zn and Se concentration profiles are observed at ~70 and 60 nm, respectively. Rapid thermal annealing results in a noticeable diffusion of Zn and Se impurities towards the SiO_2/Si interface for both types of the samples (Fig. 1c, d). However, the diffusional redistribution is more essential for the sample A.

Fig. 2 shows the XTEM images of the as-implanted and annealed samples A and B. One can see two spatially separated layers in the as-implanted sample A (Zn + Se) (Fig. 2a). No clusters are observed on the surface and in the subsurface layer up to 40 nm deep. Underneath that cluster-free region, the layer with small (2–15 nm) clusters is located in the depth range of (40–190 nm). The bigger clusters of 8–15 nm are concentrated at a depth of 80–100 nm (near the maximum of the impurity concentration – Fig. 1a). Such precipitate size distribution is typical of the clusters formed by ion implantation [14,16]. Similar features are observed for the sample B (Se + Zn) (Fig. 2b). However, the layer with the clusters is thinner (0–150 nm), and the size of clusters at the concentration maximum of embedded impurities is bigger (10–20 nm at depths of 60–100 nm in this case) in comparison with the sample A. It can be supposed that the firstly implanted Se ions prevent diffusion of the secondly implanted Zn ions to the depth of oxide film via the formation of Zn−Se bonds. This results in a higher concentration of both embedded impurities in a narrower region of SiO_2 matrix compared to the sample A. Accordingly, the larger clusters are revealed in this region.

RTA results in a structural rearrangement for both samples (Fig. 2c, d). The number of small inclusions decreases significantly, and large precipitates of regular shape appear. The size of such precipitates varies from 50 to 60 nm, and the secondary defects (stacking faults, twin boundaries) are registered inside them. It should be noted that in the case of the annealed sample A (Fig. 2c) the layer with large precipitates is located at the depth of 20–100 nm. Smaller clusters (20–40 nm) are registered in the other regions of the SiO_2 layer and even at the SiO_2/Si interface. This is in agreement with the impurity diffusional redistribution deep into the silicon dioxide layer observed in the concentration profiles of the sample A (Fig. 1c). In the case of the sample B (Fig. 2d), RTA results in the formation of larger clusters predominantly at a depth of 40–110 nm while there are no single small clusters in the other regions of oxide matrix. Segregation of impurities (presumably Se) is observed at some points of the surface for the sample B.

Fig. 3 depicts the Raman spectra of the samples A and B. The second order 2TA (transverse acoustical) phonon mode of Si substrate at $\sim 301\,cm^{-1}$ is observed in all spectra. The Raman spectra of the as-implanted samples A and B are characterized with the band at $\sim 252\,cm^{-1}$ assigned to the LO (longitudinal optical) phonon of crystalline ZnSe [5,7,17]. Thus the clusters observed in the TEM images of as-implanted samples correspond to the ZnSe nanocrystals. The TO (transverse optical) phonon line at $205\,cm^{-1}$ is probably too weak to be resolved for the geometry of our experiment [18] in the Raman spectra. It should be noted that the ZnSe band intensity is higher for the sample A than for the sample B. Based on the RBS and TEM data, the amount of the implanted species involved in clusters formation is almost similar in the samples A and B. Taking it into account the observed difference of ZnSe signal intensity in the RS spectra can be explained via the difference of crystalline quality of synthesized ZnSe NCs in the samples A and B. Based on the results of Refs [16,19], it is obvious that impurity atoms embedded in the first implantation stage should be agglomerated in the Zn or Se clusters (in the case of the samples A and B, respectively). In the second step of implantation, the implanted species should be embedded in the Zn or Se clusters already formed in the SiO_2 matrix in the first stage of implantation. According to the RS data, one can conclude that the incorporation of Se ions into the Zn clusters leads to the formation of ZnSe nanocrystals of higher crystalline quality than the incorporation of Zn ions in Se clusters. Thus, the implantation order (Zn ± Se) is more preferable for creation of high-quality ZnSe NCs in comparison with the inverted implantation order (Se ± Zn). RTA results in a slight decrease of ZnSe band intensity in the RS spectrum of the sample A. This can be explained by the formation of large nanocrystals with secondary defects during annealing as can be seen in the TEM images (Fig. 2).

Let us consider light-emitting properties of the ZnSe nanostructures. It is known that the room temperature PL spectrum of ZnSe nanostructures is typically dominated by two characteristic emission peaks. They are a near band edge (NBE) emission peak in the blue spectral range and a broad deep defect (DD) emission band in the wavelength range of 500–680 nm (green-red spectral region) [3,20]. The NBE emission is generally assigned to the excitons bound to neutral and charged acceptor and donor of different chemical nature and donor-acceptor pairs. The lines of donor-bound (I_2) and acceptor-bound excitons (I_1) in the bulk ZnSe crystals ($T = 10$ K) are observed in the energy range of (2.794–2.802) eV and (2.78–2.794) eV, respectively [21]. In the case of pure, "not-intentionally" doped ZnSe, Zn interstitials and Se vacancies can play the role of donors, and Zn vacancies can play the role of acceptors [3]. On the other hand, the deep level defect emission is mainly due to the intrinsic point defects such as vacancies, interstitials, stacking faults, and antisites [20]. Also, the green emission band was ascribed to imperfections such as dislocations and vacancies on the nanocrystal surface [22,23]. Additionally, the DD emission band can be assigned to the donor-acceptor pair (DAP) recombination mechanism involving Zn vacancies as the acceptor species and Zn interstitials as the donor species with large separation between

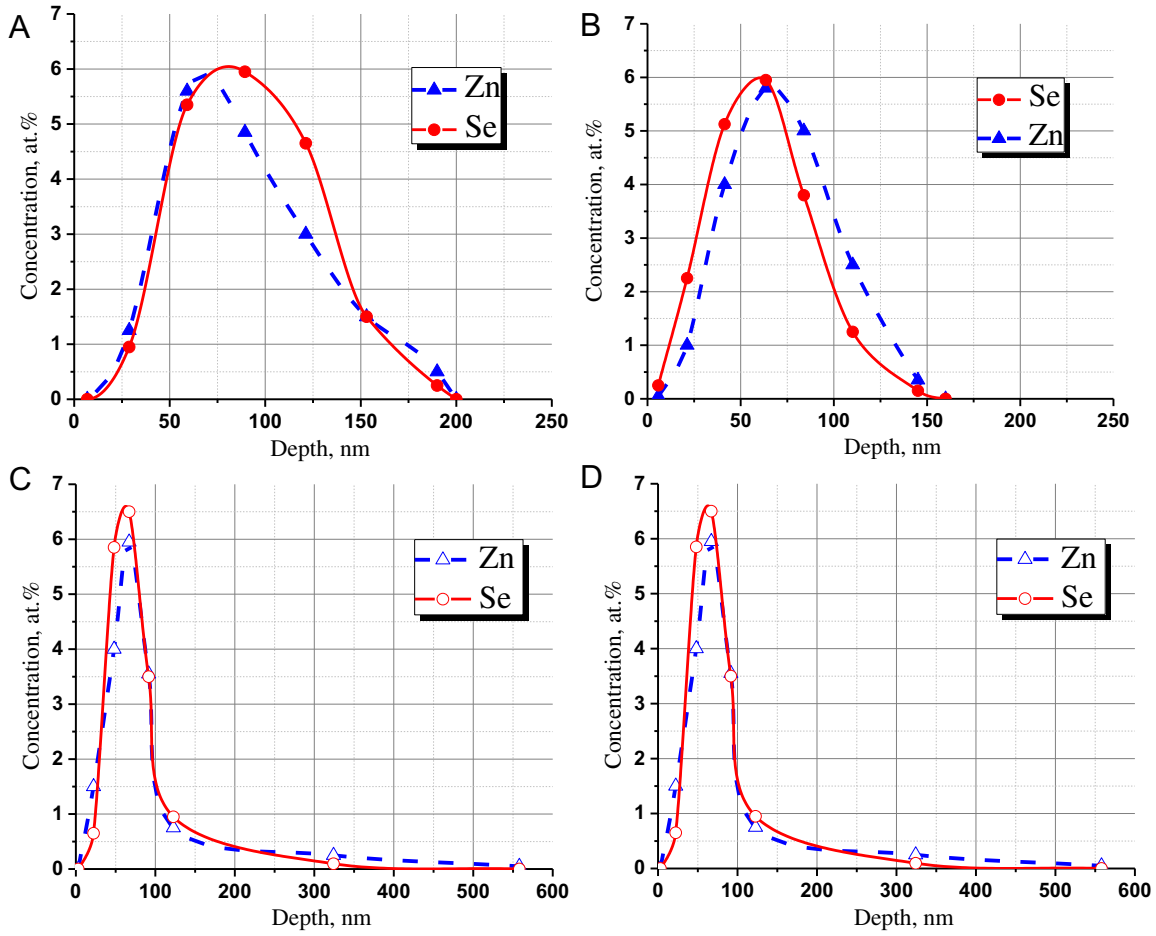

Fig. 1. Depth distributions of impurities in SiO_2 films after implantation for the as-implanted (a, b) and annealed (c, d) samples A (a, c) and samples B (b, d).

them [3,4]. It should be noted that the intensity ratio of DD and NBE emission (I_{DD}/I_{NBE}) is strongly dependent on the ZnSe growth conditions and heat treatment regimes [3].

Below, the peculiarities of the PL spectra for both sets of samples in our experiment are discussed. Fig. 4 shows the PL spectra of the as-implanted and annealed samples (A and B sets). The PL spectra of the as-implanted samples exhibit an intense blue band with the maximum at ~2.85 eV and a green band at ~2.3 eV. The blue band is related to

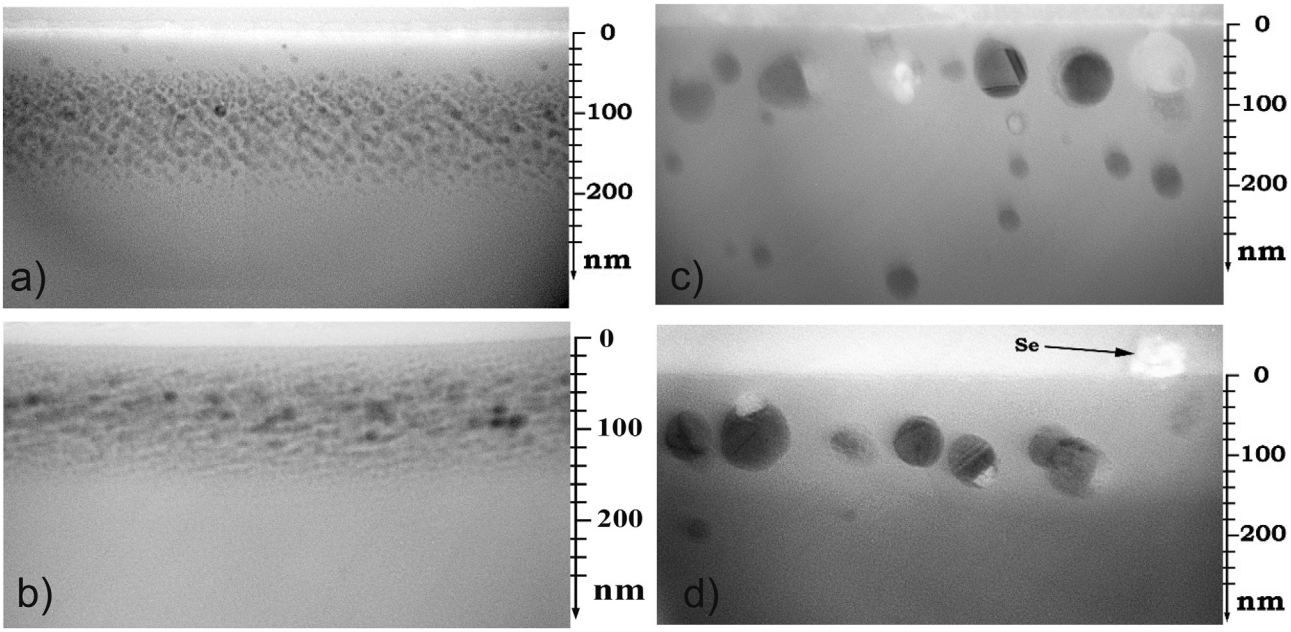

Fig. 2. Bright-field XTEM images of the as-implanted (a, b) and annealed (c, d) samples A (a, c) and B (b, d).

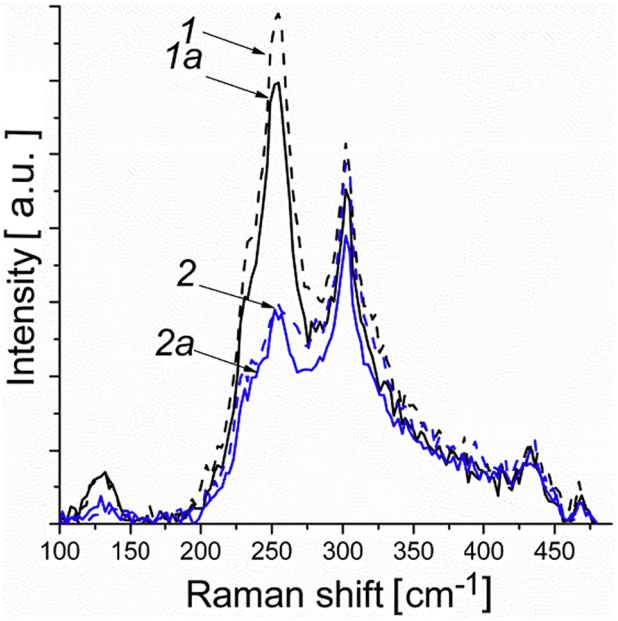

Fig. 3. Raman spectra of the as-implanted (1, 2) and annealed (1a, 2a) samples A (1, 1a) and B (2, 2a).

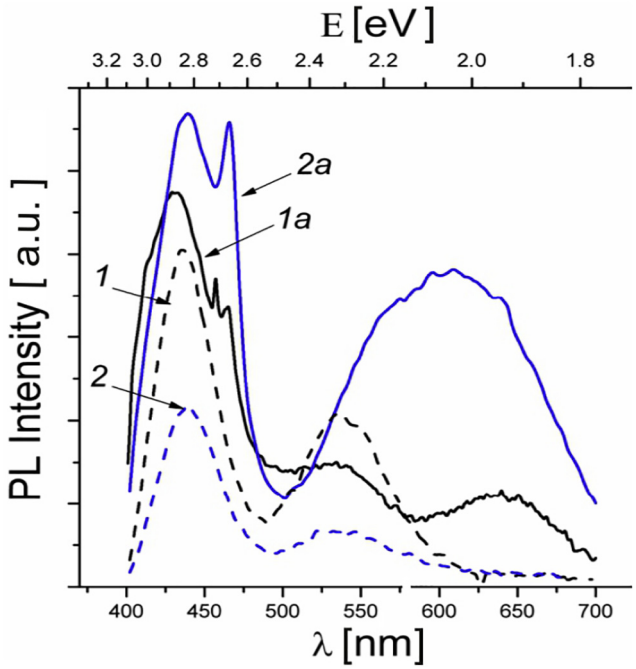

Fig. 4. PL spectra of the as-implanted (1, 2) and annealed (1a, 2a) samples A (1, 1a) and B (2, 2a).

the recombination of free and/or bound excitons (NBE band) confined in the ZnSe nanocrystals. Spectral broadening of this band is probably caused by the size distribution of nanocrystals. The maximum of the NBE bands (spectra 1 and 2 in Fig. 4) (~2.85 eV) is above the band gap energy of bulk ZnSe at RT (E_g = 2.72 eV). It reflects a blue-shift of the excitation energy of the ZnSe nanocrystals with a decreasing NCs average diameter due to the quantum-size effects [24,25]. Similar room temperature emission bands at photon energies above E_g were observed in the range 2.8–3.2 eV for ZnSe nanocrystals of different sizes embedded into the glass matrix [26] and for ZnSe NCs synthesized by a solvothermal technique [27]. The green DD band is attributed to the defect-related emission as it was mentioned above. It should be noted that the intensity ratio of DD emission to NBE emission (I_{DD}/I_{NBE}) is higher for the sample B. This is in agreement with the Raman data of 'low structural quality' of ZnSe precipitates in the sample B in comparison with those in the sample A.

RTA results in the PL intensity increase and more complicated shape of spectral bands for both types of the samples (Fig. 4). The PL intensity increase is especially noticeable for the sample B (spectrum 2a). In the case of the sample A (spectrum 1a), a blue shift of the NBE band at 2.87 eV and its extension to the high-energy side are observed after annealing. Two additional narrow lines with maxima at 2.72 eV and 2.67 eV appear in the spectrum 1a after annealing. In the case of sample B one additional line at 2.67 eV also appears after annealing, and its intensity is higher than that for the sample A. The origin of this line is most likely due to radiative decay of excitons in the largest spherical ZnSe nanocrystals observed in the XTEM images after RTA (Fig. 2c, d). In the case of ZnSe the blue-shift of PL band is negligible for the NCs with a diameter a higher than about 50 nm since the exciton Bohr radius a_B = 3.5 nm [26] is very small compared to a, i.e. $a_B < < a$ (the weak confinement regime [25]). The PL line at 2.67 eV shows, in fact, a bulk-like character. Indeed, its energy position and relatively small half-width are in agreement with those of undoped nominally pure bulk ZnSe crystals [25]. The narrow line at 2.72 eV observed in the sample B can correspond to uniformly distributed NCs of smaller sizes.

The intensity ratio of the greenish band at 550 nm (2.25 eV) to the NBE band decreases for the sample A whereas the weak red band at 650 nm (1.9 eV) appears after annealing (Fig. 4). A wide intensive band with the maximum at 2.05 eV is observed in the PL spectrum of the annealed sample B (spectrum 2a). The PL spectrum rearrangement in the long-wave range (500–650 nm) after annealing can be caused by the transformation of ZnSe nanocrystal defect structure. It should be noted that the intensity ratio I_{DD}/I_{NBE} remains higher for the sample B after annealing. This is in agreement with the RS data.

4. Conclusions

In summary, the ZnSe nanocrystals have been synthesized in the SiO_2 matrix by 'hot' implantation of Zn and Se ions. The order of Zn^+ and Se^+ ions implantation affects the structural and optical properties of synthesized nanocrystals. It determines the depth of location of the layer with nanocrystals and their size distribution. In the case of Se^+ implantation at first, the implanted species are contained in a thinner surface layer and the size of nanocrystals is bigger in comparison with the samples implanted in the opposite order.

Based on the RS data, the crystalline nature of ZnSe clusters was established for the as-implanted as well as annealed implanted samples in spite of the implantation order. However, it can be assumed from the Raman and TEM data that Se^+ implantation at first results in a more defective structure of the synthesized nanocrystals. Rapid thermal annealing leads to a significant structural rearrangement: a wide band of small clusters disappears and a layer of large separated crystallites of ZnSe is formed.

The photoluminescence data are in good agreement with the nanocrystal structural quality. The "ZnSe + SiO_2"composite exhibits blue band edge emission due to the quantum size effect and green-red deep defect emission characteristic of the ZnSe nanophase. The intensity ratio of the deep defect band to the near band edge band of ZnSe is higher for the Se implantation at first.

Acknowledgments

This research was partly supported by the Belarusian Republican Foundation for Fundamental Research, grant no. F17M-053.

References

[1] Lanlan Chen, Yang Jiang, Xinmei Liu ChunWang, Yan Chen, Jiansheng Jie, Green

chemical approaches to ZnSe quantum dots: preparation, characterisation and formation mechanism, J. Exp. Nanosci. 5 (2010) 106–117.
[2] L. Hou, C. Chen, L. Zhang, Q. Xu, X. Yang, M.I. Farooq, J. Han, R. Liu, Y. Zhang, L. Shi, B. Zou, Spin-related micro-photoluminescence in Fe^{3+} doped ZnSe nanoribbons, Appl. Sci. 7 (39) (2017) 1–10.
[3] U. Philipose, T. Xu, S. Yang, Ping Sun, Harry E. Ruda, Y.Q. Wang, K.L. Kavanagh, Enhancement of band edge luminescence in ZnSe nanowires, J. Appl. Phys. 100 (2006) 084316.
[4] Jian Wei, Kezhi Li, Jin Chena, Junzhan Zhanga, Ronghui Wua, Synthesis and photoluminescence of semiconductor ZnSe hollow microspheres by two-sourced evaporation, J. Alloys Compd. 531 (2012) 86–90.
[5] S.V. Pol, V.G. Pol, J.M. Calderon-Moreno, S. Cheylan, A. Gedanken, Facile synthesis of photoluminescence ZnS and ZnSe nanopowders, Langmuir 24 (2004) 10462–10466.
[6] D.J. Norris, N. Yao, F.T. Chamock, T.A. Kennedy, High-quality manganese-doped ZnSe nanocrystals, Nano Lett. 1 (2001) 3–7.
[7] K. Gong, D.F. Kelley, A.M. Kelly, Resonance Raman spectroscopy and electron-phonon coupling in zinc selenide quantum dots, J. Phys. Chem. C 120 (2016) 29533–29539.
[8] N. Murase, M. Gao, Preparation and photoluminescence of water-dispersible ZnSe nanocrystals, Mater. Lett. 58 (2004) 3898–3902.
[9] Yu-lu Duan, Sheng-lian Yao, Cheng Dai, Xiao-he Liu, Xu Guo-fu, Characterization of ZnSe microspheres synthesized under different hydrothermal conditions, Trans. Nonferrous Metals Soc. China 24 (2014) 2588–2597.
[10] Ling Ling Peng, Yu Hua Wang, Cheng Yan Li, Ultraviolet-blue photoluminescence of ZnSe quantum dots, J. Nanosci. Nanotechnol. 10 (2010) 2113–2118.
[11] A. Meldrum, C.W. White, L.A. Boatner, I.M. Anderson, R.A. Zuhr, E. Sonder, J.D. Budai, D.O. Henderson, Microstructure of sulphide nanocrystals formed by ion-implantation, Nucl. Inst. Methods Phys. Res. B 148 (1999) 957–963.
[12] K.Y. Gao, H. Karl, I. Grosshans, W. Hipp, B. Stritzker, Comparative study of as-implanted and pre-damaged ion-beam-synthesized ZnS nanocrystallites in SiO_2, Nucl. Inst. Methods Phys. Res. B 196 (2002) 68–74.
[13] H. Mortitz Mangold, H. Karl, Hubert J. Krenner, Site-selective ion beam synthesis and optical properties of individual CdSe nanocrystals quantum dots in SiO_2 matrix, ACS Appl. Mater. Interfaces 6 (2014) 1339–1344.
[14] H. Amekura, N. Umeda, Y. Sakuma, O.A. Plaksin, Y. Takeda, N. Kishimoto, C.H. Buchal, Zn and ZnO nanoparticles fabricated by ion implantation combined with thermal oxidation, and the defect-free luminescence, Appl. Phys. Lett. 88 (2006) 153119.
[15] J.D. Budai, C.W. White, S.P. Withrow, R.A. Zuhr, J.G. Zhu, Synthesis, optical properties, and microstructure of semiconductor nanocrystals formed by ion implantation, Mater. Res. Soc. Symp. Proc. 452 (1997) 89–98.
[16] F. Komarov, L. Vlasukova, O. Milchanin, W. Wesch, E. Wendler, J. Zuk, I. Parkhomenko, Ion-beam synthesis and characterization of narrow-gap A_3B_5 nanocrystals in Si: effect of implantation and annealing regimes, Mater. Sci. Eng. B 178 (2013) 1169–1177.
[17] H.I. Wang, W.T. Tang, L.W. Liao, P.S. Tseng, C.W. Luo, C.S. Yang, T. Koboyashi, Femtosecond laser-induced formation of wurtzite phase ZnSe nanoparticles in air, J. Nanomater. 2012 (2012) 1–6 278364.
[18] D. Nesheva, M.J. Scepanovic, S. Askrabic, Z. Levi, I. Bineva, Raman scattering from ZnSe nanolayers, Acta Phys. Pol. A 116 (2009) 75–77.
[19] X.B. Zhang, K.L. Ha, S.K. Hark, Selenium-related luminescent centers in metalorganic chemical-vapor-phase deposition grown ZnSe epilayers on GaAs, Appl. Phys. Lett. 79 (2001) 1127.
[20] A.L. Tchebotareva, J.L. Brener, S. Roorda, C.W. White, Properties of InAs nanocrystals in silicon formed by sequential ion implantation, Nucl. Inst. Methods Phys. Res. B 175–177 (2001) 187–192.
[21] G.H. Kudlek, U.W. Pohl, C.H. Fricke, R. Heitz, A. Hoffmann, J. Gutowski, I. Broser, Electronic structure and dynamical behaviour of different bound-exciton complexes in ZnSe bulk crystals, Physica B185 (1993) 325–331.
[22] H.S. Chen, S.J.J. Wang, C.J. Lo, J.Y. Chi, White-light emission from organics-capped ZnSe quantum dots and application in white-light-emitting diodes, Appl. Phys. Lett. 86 (2005) 1–3 (131905).
[23] Z. Deng, F.L. Lie, S. Shen, I. Ghosh, M. Mansuripur, A.J. Muscat, Water-based route to ligand-selective synthesis of ZnSe and Cd-doped ZnSe quantum dots with tunable ultraviolet to blue photoluminescence, Langmuir 25 (2009) 434–442.
[24] L.E. Brus, Electron–electron and electron-hole interactions in small semiconductor crystallites: the size dependence of the lowest excited electronic state, J. Chem. Phys. 80 (1984) 4403–4409.
[25] Y. Kayanuma, Quantum-size effects of interacting electrons and holes in semiconductor microcrystals with spherical shape, Phys. Rev. B 38 (1988) 9797–9805.
[26] S. Mochizuki, K. Umezawa, Optical absorption and photoluminescence of ZnSe microcrystals in a Pyrex glass matrix, J. Phys. Condens. Matter 8 (1996) 7509–7521.
[27] P. Kumar, J. Singh, M.K. Pandey, C.E. Jeyanthi, R. Siddheswaran, M. Paulraj, K.N. Hui, K.S. Hui, Synthesis, structural, optical and Raman studies of pure and lanthanum doped ZnSe nanoparticles, Mater. Res. Bull. 49 (2014) 144–150.